Available online at www.sciencedirect.com
SCIENCE DIRECT
International Journal of Mass Spectrometry 252 (2006) 61–68
International Journal of Mass Spectrometry
www.elsevier.com/locate/ijms

Instabilities of ion motion in a linear Paul trap

A. Drakoudis, M. Söllner, G. Werth*

Johannes Gutenberg University, Department of Physics, 55099 Mainz, Germany

Received 14 December 2005; received in revised form 6 February 2006; accepted 8 February 2006
Available online 29 March 2006

Abstract

We have investigated the stability properties of a linear radio frequency ion trap with cylindrical electrodes. Inside the region of stability for an ideal trap we found a number of instabilities similar to those experimentally observed in three-dimensional traps. They arise from higher order contributions to the ideal quadrupole trapping potential. The static potential for axial confinement shifts the radial ion oscillation frequencies and leads to additional instabilities.

Keywords: Ion trap; Nonlinear resonance; Multipole fields; Mass specific heating

1. Introduction

Ions stored in ion traps represent nearly ideal systems of study in a variety of fields in physics. Such fields include precision measurements of atomic transition frequencies and masses as well as the controlled manipulation of quantum states. In recent years *linear* Paul traps have been increasingly used for various kinds of experiments, ranging from lifetime measurements of long-lived metastable excited states in ions [1,2], precision hyperfine measurements leading to the development of atomic clocks in the microwave and optical domain [3,4], Coulomb crystal studies [5–7], or projects which aim to realize quantum computing schemes [8,9]. In some of these experiments the trap is considered as mere container which keeps the ion in place and details of the trapping potential and the ion motion are of little significance. In many cases, however, ion cooling to the lowest attainable temperatures is required. Then, it is of importance to deal with effects which may limit the temperature by energy pick-up from the time-varying electric trapping field.

Linear Paul traps typically consist of four metal rods symmetrically arranged as shown in Fig. 1. Two opposing rods are electrically connected and a radio-frequency field is applied to them, while the remaining two are kept at rf ground. A dc electric field may also be superimposed. In the radial direction the electric potential Φ has a quadrupolar shape:

$$\Phi(t, x, y) = (U_{\mathrm{dc}} + U_{\mathrm{ac}} \cos\ \Omega t)\frac{x^2 - y^2}{2r_0^2}. \tag{1}$$

r_0 is the distance from the rod surface to the trap center. A particle with the charge to mass ratio e/m inside this field remains trapped in the radial direction when the frequency Ω and amplitudes U_{ac} and U_{dc} (applied from pole to ground) of the rf and dc fields, respectively, are chosen in such a way that the two so-called stability parameters a and q:

$$a = \frac{4eU_{\mathrm{dc}}}{mr_0^2\Omega^2}, \qquad q = -\frac{2eU_{\mathrm{ac}}}{mr_0^2\Omega^2} \tag{2}$$

$a = a_x = -a_y, q = q_x = -q_y$ fall into a range given by the stability diagram as shown in Fig. 2. The stability parameters a and q follow from the equation of motion of a charged particle in such a time-varying field, i.e., the normalized Mathieu differential equation:

$$\frac{\mathrm{d}^2u(\tau)}{\mathrm{d}\tau^2} + (a_u - 2q_u\ \cos\ 2\tau)u(\tau) = 0 \tag{3}$$

$\tau = \Omega t/2$, $u = x, y$. Solutions of this equation are discussed in literature [10,11].

Confinement of the particles in the axial direction is provided by a static potential at the end of the rods, either by additional electrodes or by isolated segments of the main electrodes as shown in Fig. 1.

* Corresponding author.
E-mail address: werth@uni-mainz.de (G. Werth).

1387-3806/$ – see front matter © 2006 Elsevier B.V. All rights reserved.
doi:10.1016/j.ijms.2006.02.006

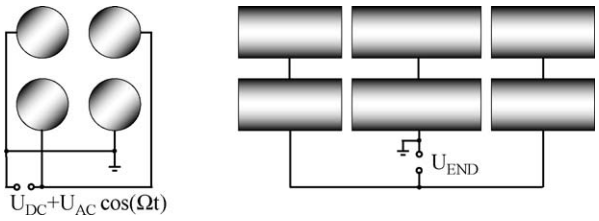

Fig. 1. Linear ion trap setup.

In the case of a single particle, stored in a perfect quadrupolar trapping potential, the ion's kinetic energy is determined by the trapping parameters and the initial conditions and remains constant in time. However, ion-ion collisions in a cloud of trapped particles, or imperfections in the trapping field may lead to ion heating and thus require detailed understanding.

The effect of such imperfections of the trapping field on the confinement properties of ions in a three-dimensional hyperbolic Paul trap was first reported by Dawson and Whetten [12], while instabilities of the ion motion in linear quadrupole devices were first observed as early as 1961 by von Busch and Paul in a mass filter [13]. Very detailed investigations on instabilities were later performed in 3D Paul traps by Alheit et al. [14,15], as well as in static Penning traps by Paasche et al. [16]. Gudjons et al. [17] used for the first time laser fluorescence from a stored ion cloud in a Paul trap to observe nonlinear resonances. Recently Douglas and Michaud have performed extensive studies of the ion motion in linear quadrupole mass filters and linear quadrupole ion traps with higher order contributions added to the quadrupole potential [18,19]. No observation of instabilities, however, has been reported in linear Paul traps so far.

Ion loss in certain operating conditions has been observed as a consequence of excessive ion heating. These conditions are characterized by the fact that in three-dimensional Paul traps the axial and radial ion oscillation frequencies in the time-averaged potential minimum, ω_z and ω_r, are related to the driving frequency, Ω, of the traps by

$$n_r\omega_r + n_z\omega_z = \Omega \tag{4}$$

The integers n_r and n_z are related to higher order contributions to the quadrupolar trapping field. Similarly in the Penning trap, operating conditions which lead to a linear dependence of the ion oscillation frequencies result in particle loss from the trap [16].

In this article we investigate the effect of trap imperfections on the stability properties of the linear Paul trap. Similar to the three-dimensional case we find instabilities in certain regions of the stability diagram. In addition the influence of the static axial confining potentials on the stability is investigated.

2. Experiment

Our ion trap consists of four cylindrical segmented rods of 6 mm diameter made from oxygen-free copper. The closest distance r_0 to the center is 2.66 mm. The length of the center segments is 15 mm, that of the outer ones 13 mm. The trap is driven by a radio frequency field at a frequency $\Omega/2\pi = 2$ MHz and variable amplitude. For axial confinement a voltage U_{END} is applied to the end caps with respect to the center segments. The trap is enclosed in a vacuum vessel at a base pressure of a few 10^{-10} mbar.

Our experiments are performed using singly ionized Ca. Ions are created by electro-ionisation of an atomic beam inside the trapping volume. Care has been taken to shield the trap electrodes from contamination with neutral Ca since this would produce imperfections in the trapping field by contact potentials. The $4S_{1/2}$–$4P_{1/2}$ resonance transition of Ca^+ at 397 nm (Fig. 3) is excited by light from a frequency doubled c.w. Ti:Sa laser and the fluorescence at the same wavelength is observed. To prevent ions from being trapped in the long-lived metastable $3D_{3/2}$ state, into which the excited $4P_{1/2}$ state may decay, we used a diode laser at 866 nm resonantly tuned to this transition for repumping. The two lasers were overlapped and aligned along the z-axis into the trap. The waist of the beam at the trap center was about 200 μm. Both lasers were stabilized against frequency drifts.

The blue laser light is tuned slightly below resonance to provide Doppler cooling of the ions. At sufficient laser power the ions' temperature, T, is reduced to a value where the Coulomb coupling parameter, Γ, defined as the ratio of the Coulomb interaction energy to the thermal energy:

$$\Gamma = \frac{1}{a_W}\frac{q^2}{4\pi\varepsilon_0}\frac{1}{k_B T} \tag{5}$$

becomes larger than 173. a_W is the mean inter-ion distance and k_B the Boltzmann constant. Then the ions form crystalline struc-

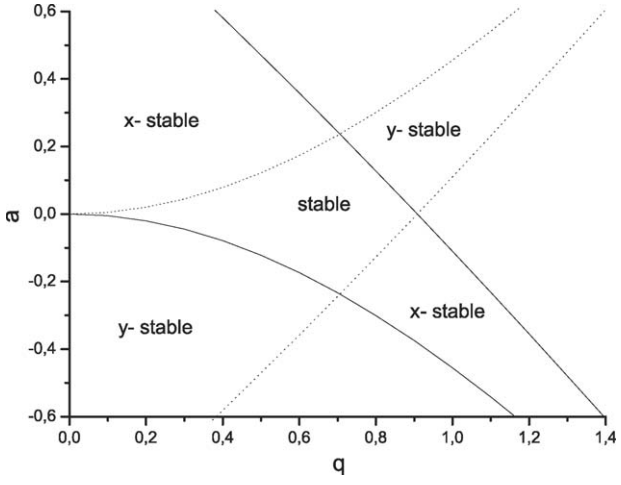

Fig. 2. Stability diagram for an ideal linear Paul trap.

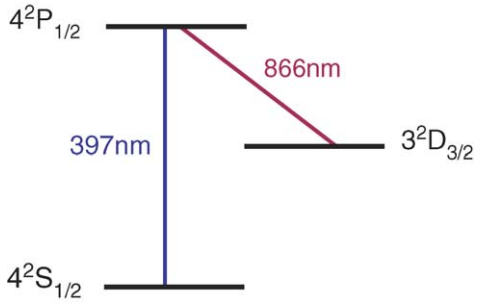

Fig. 3. Relevant $^{40}Ca^+$ level scheme.

Fig. 4. Spatially resolved observation of four ions as a cloud and as a crystallized structure.

tures [20] which arrange themselves symmetrically around the trap center [7,21,22]. In the case of a few ions they form a linear string along the trap axis with individual ions spatially resolved when using a CCD camera for fluorescence detection (Fig. 4).

We found that for our investigations on instabilities it was easier to monitor the total fluorescence from the trapped ions with a photomultiplier rather than observing the behavior of ion crystals. We therefore set the laser detuning and power to such values that the ion cloud was cooled but not crystallized and integrated the fluorescence for 500 ms at each data point. Typical ion numbers were around 10 which resulted in a detected fluorescence count rate of about 4000 s^{-1}. The ion fluorescence was monitored at different operating parameters of the linear trap. To this end, either the rf amplitude of the driving field was set to a given value (corresponding to a certain value of the stability parameter q) while the dc voltage, corresponding to the stability parameter a, was scanned across the trap or vice versa.

In order to determine the values of a and q, at which nonlinear resonances occur, it was not sufficient to measure the amplitude of the applied voltages since the uncertainty might be rather large, particularly in the amplitude of the 2 MHz rf voltage. Instead we measured the motional eigenfrequencies of the ions in the trap potential in the neighbourhood of the nonlinear resonances. According to the solution of the Mathieu equation of motion they are related to the stability parameters a and q by

$$\omega_{u,n} = \left| n + \frac{\beta_u(q_u, a_u)}{2} \right| \Omega \tag{6}$$

$u = x, y, n = 0, 1, 2, \ldots$ and β_u is a function of a_u, q_u [10,11]:

$$\beta_u^2 = a_u + \frac{q_u^2}{(2+\beta_u)^2 - a_u - \frac{q_u^2}{(4+\beta_u)^2 - a_u - \cdots}} + \frac{q_u^2}{(2-\beta_u)^2 - a_u - \frac{q_u^2}{(4-\beta_u)^2 - a_u - \cdots}} \tag{7}$$

which for $|a_u, q_u| \ll 1$ can be approximated by $\beta_u^2 = a_u + (q_u^2/2)$.

3. Results

For certain combinations of a and q a decrease in the fluorescence count rate was observed as shown in Fig. 5. This is the result of an expansion of the ion cloud when it gains energy from the trapping field due to nonlinearities in the trapping potential as will be outlined below. The shape and amplitude of these nonlinear resonances depend on the direction of the voltage scan (see Fig. 6). As is clear from Figs. 5 and 6 the ions were not lost from the trap when passing through a resonance. The width of the resonances is typically in the range of $\delta a, \delta q \simeq 10^{-4}$. Depending on the value of the storage parameter this results in relative linewidths of about $\delta a/a \leq 10^{-3}$, $\delta q/q \leq 10^{-3}$, respectively.

We measure the motional frequencies by application of an additional weak radio frequency field applied to the trap electrodes in a dipolar way. When we scan the frequency ω of this field we can resonantly excite the ions' motion. It results in a decrease of the observed fluorescence

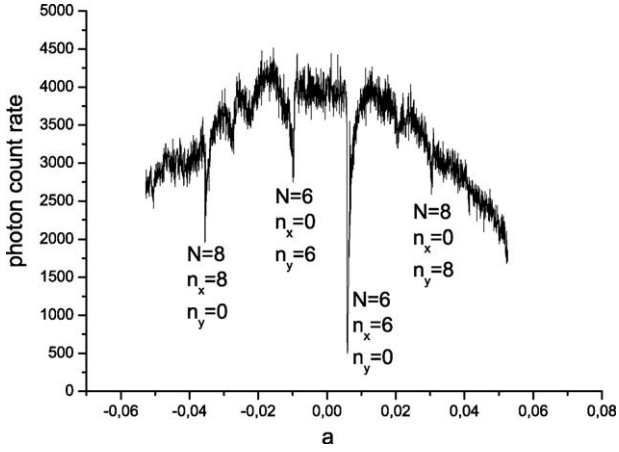

Fig. 5. Observed minima in the fluorescence count rate at different values of the stability parameter a ($q = 0.425$).

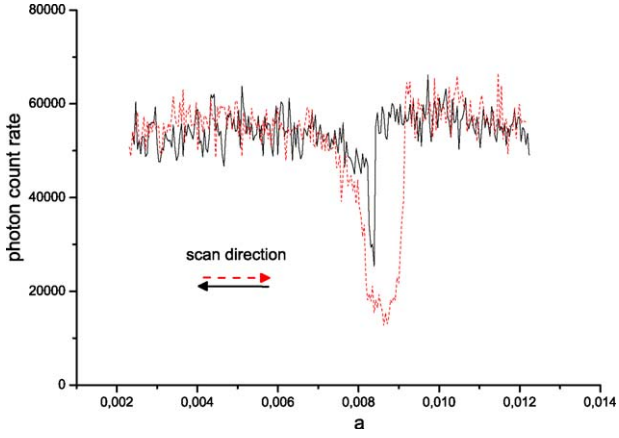

Fig. 6. Shape and amplitude of a nonlinear resonance for a large number of ions ($n \simeq 100$) as function of scan direction ($q = 0.472$).

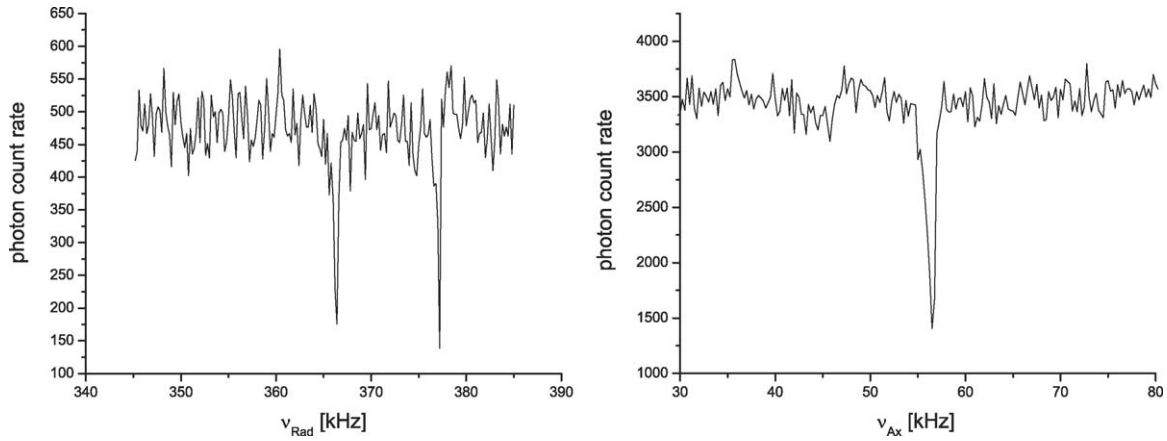

Fig. 7. Radial (left) and axial (right) excitation of the secular ion oscillation frequencies. The double structure of the radial excitation arises from different potential depths in x- and y-direction at $a \neq 0$. In the left picture the stability parameters $q = 0.491$ and $a = 0.003$ have been determined from the resonance frequencies. The axial resonance was measured at $q = 0.456$ and $U_{\mathrm{END}} = 25$ V. The two data sets were recorded for different ion numbers.

since the ion cloud expands under excitation. Fig. 7 shows examples.

The axial oscillation frequency is determined by the dc confining voltage at the outer trap segments U_{END}. Given that the distance of these segments from the trap center is 7.5 mm we can reasonably assume that the potential distribution across the ion cloud with a typical length of a few 10 μm can be considered as harmonic in the axial direction. The radial dependence of this potential follows from Laplace's equation. Considering the symmetry of the trap in x- and y-direction we have:

$$\Phi_{ax}(x, y, z) = \frac{\kappa U_{\mathrm{END}}}{d_0^2}\left(z^2 - \frac{x^2 + y^2}{2}\right) \tag{8}$$

d_0 is the distance from the axial trap center to the end electrodes [23,24]. Here a factor κ is introduced which depends on the trap's geometry and can be determined experimentally. The axial oscillation frequency then is given by

$$\omega_z = \sqrt{\frac{2\kappa e U_{\mathrm{END}}}{m d_0^2}} \tag{9}$$

The radial components of the axial potential have to be added to the radial quadrupole potential and lead to modified equations of motion:

$$\ddot{x} + \frac{e}{m}\left[\frac{U_{\mathrm{dc}} + U_{\mathrm{ac}}\cos(\Omega t)}{r_0^2} - \frac{\kappa U_{\mathrm{END}}}{d_0^2}\right] x(t) = 0,$$

$$\ddot{y} + \frac{e}{m}\left[\frac{-U_{\mathrm{dc}} - U_{\mathrm{ac}}\cos(\Omega t)}{r_0^2} - \frac{\kappa U_{\mathrm{END}}}{d_0^2}\right] y(t) = 0 \tag{10}$$

They can be cast into the standard Mathieu equation using modified stability parameters:

$$\tilde{a}_x = \frac{4eU_{\mathrm{dc}}}{mr_0^2\Omega^2} - \frac{4e\zeta U_{\mathrm{END}}}{mr_0^2\Omega^2}, \qquad \tilde{a}_y = -\frac{4eU_{\mathrm{dc}}}{mr_0^2\Omega^2} - \frac{4e\zeta U_{\mathrm{END}}}{mr_0^2\Omega^2},$$

$$\tilde{a}_z = \frac{8\kappa e U_{\mathrm{END}}}{m d_0^2\Omega^2}, \quad q = -\frac{2eU_{\mathrm{ac}}}{mr_0^2\Omega^2}, \quad \tau = \frac{\Omega t}{2}, \quad \zeta = \frac{\kappa r_0^2}{d_0^2} \tag{11}$$

When we replace the parameters β in Eq. (6) by new ones ($\tilde{\beta}$) considering the change in a by the axial potential we find for the new fundamental radial oscillation frequencies:

$$\tilde{\omega}_x = \frac{\Omega}{2}\tilde{\beta}_x = \sqrt{\omega_x^2 - \frac{1}{2}\omega_z^2} \simeq \frac{\Omega}{2}\sqrt{\frac{q^2}{2} + a_x - \frac{1}{2}\tilde{a}_z},$$

$$\tilde{\omega}_y = \frac{\Omega}{2}\tilde{\beta}_y = \sqrt{\omega_y^2 - \frac{1}{2}\omega_z^2} \simeq \frac{\Omega}{2}\sqrt{\frac{q^2}{2} + a_y - \frac{1}{2}\tilde{a}_z},$$

$$\omega_z = \frac{\Omega}{2}\sqrt{\tilde{a}_z} \tag{12}$$

As the trapping potential contains higher order potential contributions the excitation resonances are those of a driven anharmonic oscillator. Depending on the size and sign of these contributions they show asymmetries and depend on the frequency scan direction of the excitation field. This is a well-known behavior and is discussed in detail by Landau and Lifschitz [25]. Fig. 8 shows an example for one radial resonance. Because of the asymmetry and the directional dependence, accurate determination of the oscillation frequencies is difficult. We obtain the proper values by measuring the resonances at different excitation amplitudes and extrapolation to zero field strength. From these values the stability parameters a and q are determined. Also from measurements at different axial potentials the geometrical factor κ (see Eq. (9)) can be determined. For our electrode configuration we obtain $\kappa = 0.064$.

According to Eq. (12) the axial confining potential shifts the radial frequencies. In order to verify this we measured the motional frequencies for a defined radial potential at several end cap voltages U_{END}. The expected frequency shift is shown in Fig. 9 and agrees well with the observation.

We examined the effect of the axial potential on the instabilities. To this end we scanned the rf voltage for different axial potentials across the stability region while the parameter a was set to zero. This particular choice of a is due to the reduced number of resonances expected from theory (see below). Furthermore

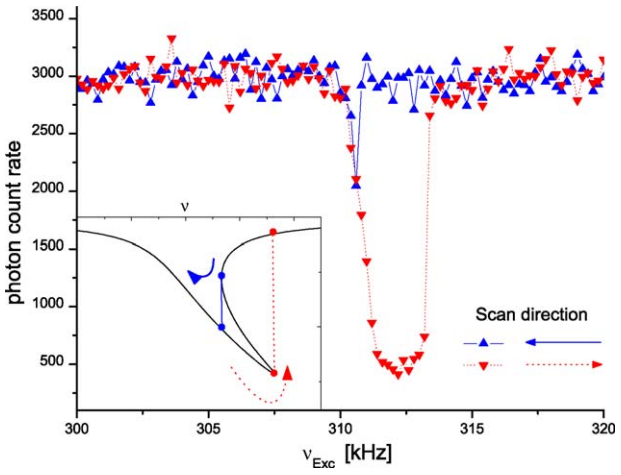

Fig. 8. High resolution scan of one of the radial ion oscillation frequencies taken at different scan directions and constant excitation amplitude (U_{EXC} = 750 mV$_{p-0}$). The insert shows the qualitative expectation from a driven anharmonic oscillator for an octopole potential contribution following Landau and Lifschitz [25].

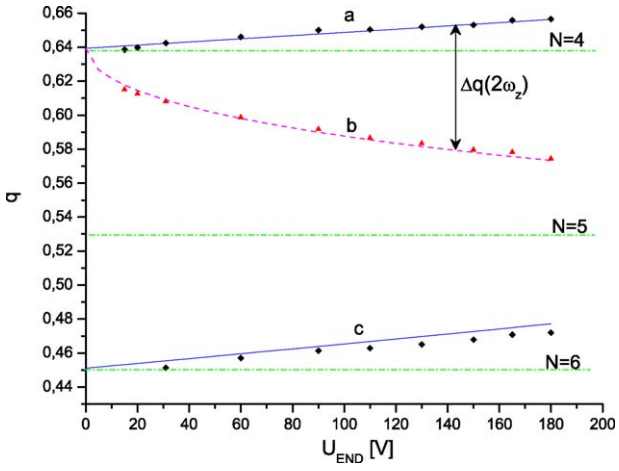

Fig. 10. Position of the observed nonlinear resonances ($N = 4$ and 6) as a function of the applied axial voltage. The purely radial coupling resonances ((a) and (c)) are shifted by the radial components of the axial potential. In addition a new instability (at $N = 4$) which couples to the axial oscillation shows up (b). The horizontal dashed lines mark the expected q-values for instabilities of the orders $N = 4$, 5 and 6 for a linear quadrupole mass filter (see below).

the radial motional frequencies for the x- and the y-directions then have the same value. Therefore any effect caused by the axial potential should be clearly evident. In the scanned region we observed three nonlinear resonances. Their positions q as a function of the applied axial voltage are shown in Fig. 10. Two of the resonances ((a) and (c)) shift to higher values of q with increasing axial voltage. They arise from purely radial coupling and can be assigned to contibutions from an octopole ($N = 4$) and a dodecapole ($N = 6$) potential, respectively. The solid lines in Fig. 10 show the potential dependence according to Eq. (12) and are in agreement with the experimentally observed shifts. Thus, the static radial components of the axial potential in effect result in reduction of the applied radial potential. Here, we would like to note, that due to the strength of the purely radial coupling resonance for $N = 4$, the ions were lost from the trap. Because of the observed narrow linewidths, however, it appears reasonable to assume the center of the resonance at the position of the ion loss itself.

In addition we found an instability which shifts to lower values of q with increasing axial potential (b). It arises from additional coupling to the axial motion at twice the axial frequency. This is seen in a comparison of the experimental data with the calculated positions in q for this kind of coupling (dashed line).

We systematically varied the stability parameters a and q in a large area of the stability diagram, while the endcap voltages U_{END} were kept at a fixed value. This lead to the observation of a number of fluorescence minima. Their positions in the stability diagram are shown in Fig. 11.

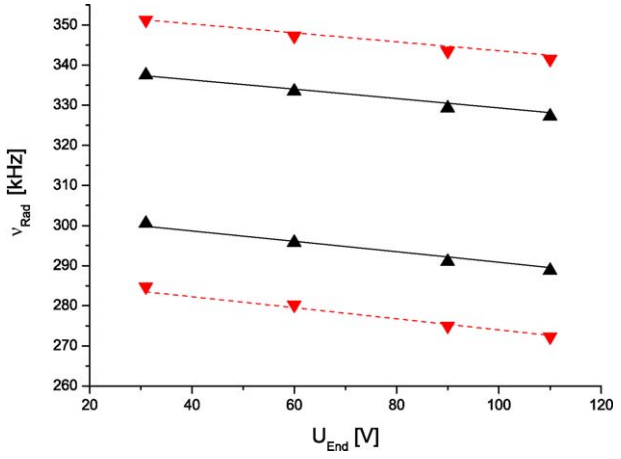

Fig. 9. Shift of the radial frequencies by the axial confining potential U_{END}. The frequencies have been measured for two different radial trapping potentials. The rf amplitude in both cases is U_{ac} = 101 V, while the static voltage U_{dc} was set to −1 V (▲) and −2 V (▼), respectively. The lines show the expected frequency shift for the applied potentials.

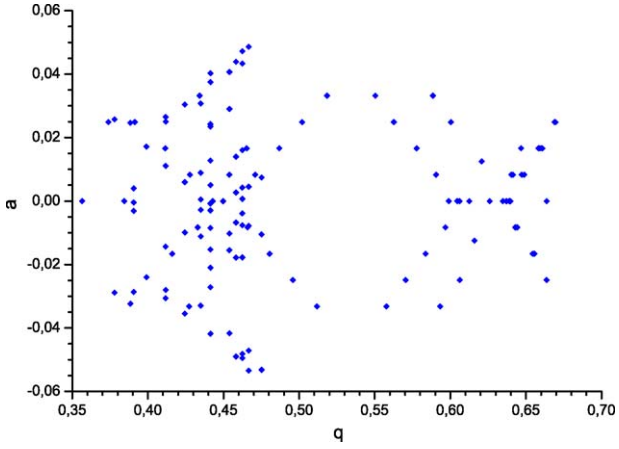

Fig. 11. Observed minima in the ion density at various values of the stability parameters a and q of the linear Paul trap at an endcap voltage U_{END} = 30 V. Below $q = 0.35$ no minima could be observed, above $q = 0.7$ loading of the trap was not efficient enough.

4. Discussion

The condition for instabilities of the ion motion in perturbed trapping potentials has been derived by Wang et al. using perturbation theory [26]. It is given for 3D potentials by Eq. (4), while for 2D potentials it reads:

$$n_x\omega_x + n_y\omega_y = \Omega \tag{13}$$

The sum of the integers n_x and n_y

$$|n_x| + |n_y| = N \tag{14}$$

gives the order of the perturbing potential when it is described by a series expansion in cylindrical coordinates:

$$\Phi_{\text{Real}}(r,\phi,t) = U(t)\sum_{k=0}^{\infty} c_k \left(\frac{r}{r_0}\right)^k \cos(k(\phi-\varepsilon_k)) \tag{15}$$

c_k denotes the strength of the potential contribution. In principle, a contribution of the order k can cause nonlinear resonances of the orders $N = k, k-2, k-4, \ldots$ However, resonances of a certain order are mainly caused by the corresponding potential order. For $k = 2$ we have the ideal quadrupole potential. The leading lower terms in Cartesian coordinates are given by

$$\Phi_3 = \frac{c_3}{r_0^3}(x^3 - 3xy^2), \qquad \Phi_4 = \frac{c_4}{r_0^4}(x^4 - 6x^2y^2 + y^4),$$
$$\Phi_5 = \frac{c_5}{r_0^5}(x^5 - 10x^3y^2 + 5xy^4) \tag{16}$$

Fig. 12 shows the expected instabilities in the stability diagram for several higher order contributions.

In Fig. 13 we compare our experimental observations to the theoretical expectations. The unstable operating points follow closely the calculated lines. The labelling of the lines is $N/n_x/n_y$. Thus we observe instabilities arising from octopole

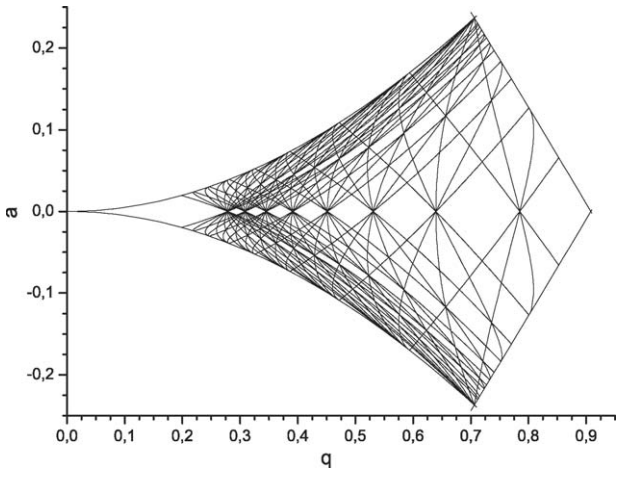

Fig. 12. Theoretical stability diagram of a linear quadrupole mass filter. Inside the boundary of the stable region lines are drawn which correspond to expected instabilities of the ion motion due to perturbing trapping potentials of order N according to Eqs. (13) and (14). All instabilities arising from a given order N meet at one point at the q-axis. Shown are instabilities ranging from $N = 3$ (right) to $N = 10$ (left).

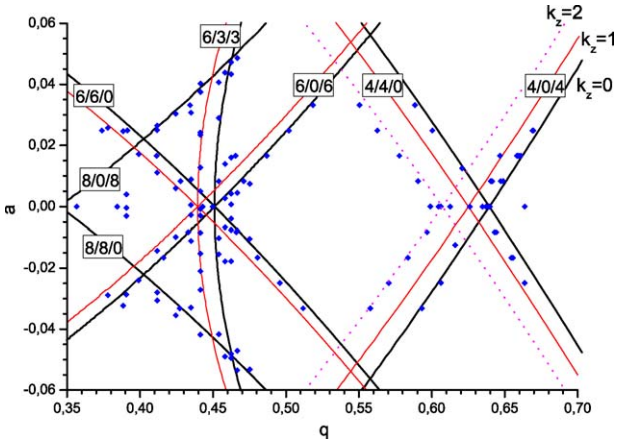

Fig. 13. Comparison of experimentally observed instabilities to expectations from Eq. (13) and the modified condition for nonlinear resonances Eq. (17).

($N = 4$), dodecapole ($N = 6$) and hexadecapole ($N = 8$) perturbations. We note that we observe (with the exception of the (6/3/3) resonance) only instabilities at which one of the integers n_x or n_y is 0. The bold lines in Fig. 13 correspond to pure radial resonances coupled to the trapping field. The normal lines indicate instabilities where in addition the axial oscillation is coupled to the radial one. In case of the $N = 4$ instability we find also some instabilities which correspond to the coupling of $2\omega_z$ to the axial frequency (dotted). As a result the condition for instabilities in a linear Paul trap, as stated in Eq. (13) has to take into account the influence of the axial potential and must then be written as

$$n_x\tilde{\omega}_x + n_y\tilde{\omega}_y = \Omega - k_z\omega_z, \quad k_z = 0, 1, 2, \ldots \tag{17}$$

Some pronounced instabilities occurring near $a = 0$ and $q = 0.4$ could not be assigned. They would correspond approximately to instabilities arising from $N = 7$ perturbations. The symmetry of the electrode configuration, however, would allow only non-zero perturbations for even N.

In order to obtain at least approximate values for the size of the perturbing higher order potentials we calculated ion trajectories for our geometry using the simulation program SIMION. From the observed amplitude of the oscillations at different ion energies we obtained the following values for the coefficients c_k in the series expansion of the potential (normalized to $c_2 = 1$):

$$c_4 = 0.061, \qquad c_6 = -0.022, \qquad c_8 = 0.003$$

These values correspond approximately to the strength of the observed instabilities of the corresponding orders. However, calculations for an ideal linear quadrupole mass filter with cylindrical electrodes and the same $R/r_0 = 1.13$ ratio (R the radius of the electrode and r_0 the shortest distance from the trap center to the electrodes) give a value $c_6 \simeq 0.001$ for the hexapole contribution, whereas c_4 and c_8 do not contribute, due to the potential symmetry [27,28].

The observation of instabilities in the ion motion in a linear Paul trap follows closely what was expected from detailed measurements and calculations in three-dimensional Paul traps as well as early observations in linear Paul mass filters. The

influence of the static axial confining potential on the radial ion motion, however, has so far not yet been considered. It shifts the oscillation frequencies and leads to additional instabilities. This might be of importance for mass spectrometry using linear Paul traps if, for example, ions created inside the trap by fragmentation of parent ions happen to fall into a region of the stability diagram where instabilities are likely to occur.

One possible application for mass spectrometry in linear Paul traps is the purification of mass samples resulting from the relatively simple and precise control of the axial potential. By varying the voltages applied for the axial confinement it is possible to tune these additional resonances to unwanted masses and by this concentrate the analyte ions in the sample. In a three-dimensional Paul trap the removal of unwanted isotopes using instabilities by variation of the working parameters a and q was demonstrated first by Alheit [29] and Alt [30].

In experiments on cooled stored ions, nonlinear resonances may lead to excessive heating and thus may prevent the achievement of very low temperatures.

The question remains about the origin of the instabilities. Trap imperfections, as stated above, are generally considered to be the main source. Calculations [31] show that space charge effects in Paul traps on the position of ion oscillation frequencies become significant only when the space charge density is of the order of 10^5 cm^{-3}. Since we generally work with small ion numbers, of the order of 10, we did not originally consider this to be a detectable contribution to the occurrence of instabilities. This, however, might not be the case. In one of our runs we lost some ions from the trap when scanning the voltage across a nonlinear resonance. We found that the fluorescence count rate was quantized and could thus determine the trapped ion number accurately. The decrease of fluorescence at the nonlinear resonance remained visible until the ion number was reduced to three and then vanished completely (Fig. 14). This somewhat surprising observation may be explained by the fact that the ion cloud was cooled by the red detuned laser light and that at the smallest ion number a phase transition to a crystallized state occurred. Our photomultiplier based detection system would not be able to distinguish between a small ion cloud and a crystal. A crystal, well aligned along the trap axis, might not feel the influence of trap imperfections. This question requires further investigations

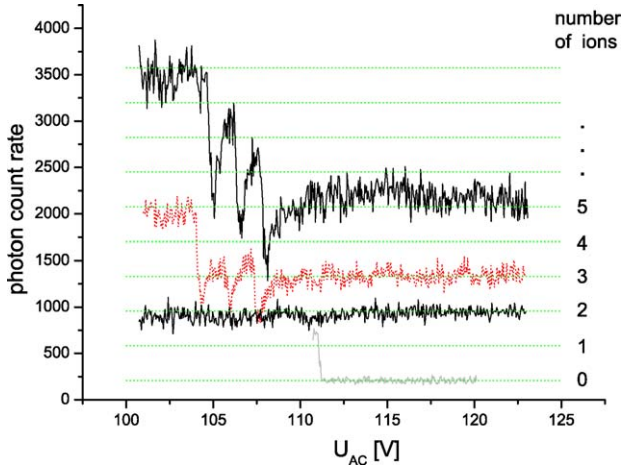

Fig. 14. Nonlinear resonance ($N = 6$) at small ion numbers. The ion number (horizontal lines) is derived from the quantized fluorescence count rate. The multiple peak structure arises from a partially compensated patch potential ($a \simeq 0$).

Acknowledgements

Our experiments were supported by the Deutsche Forschunggemeinschaft and by a grant from the European Union (FP6-2002-IST-C, Proj. 003772). We like to thank H. Leuthner for his helpful hands setting up the experiment.

References

[1] M. Block, O. Rehm, P. Seibert, G. Werth, Eur. Phys. J. D 7 (1999) 461.
[2] P.A. Barton, C.J.S. Donald, D.M. Lucas, D.A. Stevens, A.M. Steane, D.N. Stacey, Phys. Rev. A 62 (2000) 032503.
[3] R.L. Tjoelker, J.D. Prestage, L. Maleki, Proceedings of the 31st Annual Time and Time Interval (PTTI) Meeting, vol. 597 (1999).
[4] S.A. Diddams, Th. Udem, J.C. Bergquist, E.A. Curtis, R.E. Drullinger, L. Hollberg, W.M. Itano, W.D. Lee, C.W. Oates, K.R. Vogel, D.J. Wineland, Science 293 (2001) 825.
[5] M.G. Raizen, J.M. Gilligan, J.C. Bergquist, W.M. Itano, D.J. Wineland, Phys. Rev. A 45 (1992) 6493.
[6] H.C. Nägerl, D. Leibfried, F. Schmidt-Kaler, J. Eschner, R. Blatt, Opt. Express 3 (1998) 89.
[7] M. Drewsen, C. Brodersen, L. Hornekær, J.S. Hangst, J.P. Schiffer, Phys. Rev. Lett. 81 (1998) 2878
L. Hornekær, N. Kjærgaard, A.M. Thommesen, M. Drewsen, Phys. Rev. Lett. 86 (2001) 1994.
[8] D. Leibfried, B. DeMarco, V. Meyer, M. Rowe, A. Ben-Kish, M. Barrett, J. Britton, J. Hughes, W.M. Itano, B.M. Jelenkovic, C. Langer, D. Lucas, T. Rosenband, D.J. Wineland, J. Phys. B 36 (2003) 599.
[9] F. Schmidt-Kaler, H. Häffner, S. Gulde, M. Riebe, G.P.T. Lancaster, T. Deuschle, C. Becher, W. Hänsel, J. Eschner, C.F. Roos, R. Blatt, Appl. Phys. B 77 (2003) 789.
[10] N.W. McLachlan, Theory and Application of Mathieu Functions, Oxford University Press, London, 1951.
[11] J. Meixner, F.W. Schäfke, Mathieusche Funktionen und Sphäroidfunktionen, Springer, Berlin/Heidelberg, 1954.
[12] P.H. Dawson, N.R. Whetten, Int. J. Mass Spectrom. Ion Phys. 2 (1969) 45.
[13] F.v. Busch, W. Paul, Z. Phys. 164 (1961) 588.
[14] R. Alheit, C. Hennig, R. Morgenstern, F. Vedel, G. Werth, Appl. Phys. B 61 (1995) 277.
[15] R. Alheit, S. Kleineidam, F. Vedel, M. Vedel, G. Werth, Int J. Mass Spectrom. Ion Proc. 154 (1996) 155.
[16] P. Paasche, C. Angelescu, S. Ananthamurthy, D. Biswas, T. Valenzuela, G. Werth, Eur. Phys. J. D 22 (2003) 183.
[17] T.E. Gudjons, P. Seibert, G. Werth, Appl. Phys. B 65 (1997) 57.
[18] D.J. Douglas, N.V. Konenkov, Rapid Commun. Mass Spectrom. 16 (2002) 1425.
[19] A.L. Michaud, A.J. Frank, C. Ding, X. Zhao, D.J. Douglas, J. Am. Soc. Mass Spectrom. 16 (2005) 835.
[20] J.P. Schiffer, Phys. Rev. Lett. 70 (1993) 818.
[21] T. Schätz, U. Schramm, D. Habs, Nature 412 (2001) 717
G. Birkl, S. Kassner, H. Walther, Nature 357 (1992) 310.
[22] M. Block, A. Drakoudis, H. Leuthner, P. Seibert, G. Werth, J. Phys. B 33 (2000) L375.
[23] M.G. Raizen, J.M. Gilligan, J.C. Bergquist, W.M. Itano, D.J. Wineland, Phys. Rev. A 45 (1992) 6493.
[24] Drewsen and Brøner give an alternative way for the description of stable confinement in a linear Paul trap. In particular they define one parameter, a, for confinement in all three dimensions. M. Drewsen, A. Brøner, Phys. Rev. A 62 (2000) 045401.

[25] L.D. Landau, E.M. Lifschitz, Mechanics, 3rd ed., Pergamon Press, New York, 1960
L.D. Landau, E.M. Lifschitz, Lehrbuch der theoret. Physik, Bd. 1, 12. Aufl. (Akademie Verlag Berlin, 1987).
[26] Y. Wang, J. Franzen, K.P. Wanczek, Int. J. Mass Spectrom. Ion Proc. 124 (1993) 125.
[27] D.R. Denison, J. Vac. Sci. Technol. 8 (1971) 266.
[28] D.J. Douglas, N.V. Konenkov, Rapid Commun. Mass Spectrom. 16 (2002) 1425.
[29] R. Alheit, K. Enders, G. Werth, Appl. Phys. B 62 (1996) 511.
[30] W. Alt, M. Block, V. Schmidt, T. Nakamura, P. Seibert, X. Chu, G. Werth, J. Phys. B 30 (1997) L677.
[31] F. Vedel, Int. J. Mass Spectrom. Ion Proc. 106 (1991) 33.